Bismuth Decorated Honeycomb-like Carbon Nanofibers: An Active Electrocatalyst for Construction of Sensitive Nitrite Sensor

Fengyi Wang , Ye Li , Chenglu Yan , Qiuting Ma , Xiaofeng Yang * , Huaqiao Peng , Huiyong Wang , Juan Du * , Baozhan Zheng * , Yong Guo

Posted Date: 21 April 2023

doi: 10.20944/preprints202304.0660.v1

Keywords: nitrite sensor; honeycomb-like carbon nanofibers; Bi nanoparticles; nitrite detection

Article

Bismuth Decorated Honeycomb-like Carbon Nanofibers: An Active Electrocatalyst for Construction of Sensitive Nitrite Sensor

Fengyi Wang [1,2], Ye Li [2], Chenglu Yan [3], Qiuting Ma [2], Xiaofeng Yang [1,*], Huaqiao Peng [3], Huiyong Wang [4], Juan Du [2,*], Baozhan Zheng [2,*] and Yong Guo [2]

[1] Institute of Quality Standard and Testing Technology for Agro-products of Sichuan Academy of Agricultural Sciences, Chengdu 610066, China
[2] College of Chemistry, Sichuan University, No. 29 Wangjiang Road, Chengdu 610064, China
[3] The Second Research Institute of Civil Aviation Administration of China, Chengdu 610041, China
[4] College of Chemistry and Chemical Engineering, Henan Normal University, Henan 453002, China
* Correspondence: yangxiaofeng_cd@sina.com (X.Y.); dujuanchem@scu.edu.cn (J.D.); zhengbaozhan@scu.edu.cn (B.Z.)

Abstract: Existence of carcinogenic nitrite in food has attracted much attention, however, it is still a challenge to develop nitrite sensor with higher sensitivity and selectivity to enlarge its applications in daily life. Herein, one-dimensional honeycomb-like carbon nanofibers (HCNFs) were synthesized with an electrospun technology, and its specific structure enables the controlling growth and highly dispersed bismuth nanoparticles (Bi NPs) on its surface, which endows the obtained Bi/HCNFs with excellent electrocatalytic activity toward nitrite oxidation. By modifying Bi/HCNFs on screen-printed electrode, the constructed Bi/HCNFs electrode (Bi/HCNFs-SPE) can be used for nitrite detection in one drop of solution, and exhibits higher sensitivity (1269.9 μA mM^{-1} cm^{-2}) in a wide range of 0.1~800 μM with lower detection limit (19 nM). Impressively, the Bi/HCNFs-SPE has been successfully used for nitrite detection in food and environment samples, the satisfactory property and recovery indicates its feasibility in further practical applications.

Keywords: nitrite sensor; honeycomb-like carbon nanofibers; Bi nanoparticles; nitrite detection

1. Introduction

With the development of modern technology, people are increasingly aware of the importance of food safety for health, because the abuse of common food additives, such as nitrite, will bring a great threat to human health [1,2]. On one hand, the excessive uptake of nitrite can react with amines under acidic conditions and form nitrosamine carcinogens, which will result in cancer, hypertension and neurodegenerative diseases [3,4]. In addition, nitrite can also interact with hemoglobin, the generated methemoglobin can inhibit the ability of blood to carry oxygen, leading to serious methemoglobinemia [5]. On the other hand, nitrite, as a common water-soluble nitrogenous compound, is ubiquitous within natural environment, which will also lead to water pollution and eutrophication during nitrogen cycling [6]. Notably, the World Health Organization (WHO) has stipulated that the maximum limit of nitrite concentration is 3 mg L^{-1} in drinking water [7]. Therefore, it is urgent to develop effective analytical techniques for nitrite identify and quantitative detection precisely.

Up to now, kinds of methods based on chemiluminescence [8], fluorescence [9,10], ion chromatography [11], colorimetric method [12], and electrochemistry [1,13,14] have been explored extensively for nitrite detection, while most of these methods usually suffer from relatively expensive instrument, time-consuming operation process, toxic chemical reagent, which greatly hinders their

Preprints (www.preprints.org) | NOT PEER-REVIEWED | Posted: 21 April 2023 doi:10.20944/preprints202304.0660.v1

widely applications. Comparing with these methods, the electrochemical technology has been proved to be one of the promising methods because it can be easily miniaturized and constructed cost-effectively. It is well known that the composition and morphology of catalyst materials can greatly influence the performance of electrochemical sensor, including sensitivity, selectivity, stability and reproducibility, etc. Therefore, the design and preparation of high-performance electrocatalysts is the premise to construct electrochemical sensors for nitrite detection with excellent properties.

Our previous researches have demonstrated that Bi-based materials possess high affinity for nitrogen, which therefore greatly boosts the nitrogen reduction rate [15,16]. Thus, these Bi-based materials have been widely used as electrocatalysts to catalyze the reduction of nitrite and nitrate to generate ammonia [17]. Inspired by these, we speculate that Bi-based nanomaterials will also have good performance in constructing electrochemical sensor for nitrite detection, but there are few reports in this area. Nevertheless, Bi as metal with semiconducting properties; its poor electrical conductivity will impedes its further applications in electrochemistry [18]. To overcome this disadvantage, conductive carbon materials (such as carbon nanofibers [19], carbon nanotubes [20], graphene [21] et.al) have been selected as the substrates to synthesis Bi-based nanocomposites, which can greatly improve the intrinsic electrical conductivity. In this context, porous carbon nanofibers (PCNFs) have appealed to tremendous concern in view of their outstanding features of high conductivity, large specific surface area, and environmental-friendly properties [1]. To date, PCNFs are generally fabricated by corrosive chemical agents such as KOH or HNO_3, yet there are unsafe and non-environmental friendly in large-scale industrial manufacturing [22,23]. In terms of the template method, the main route of conventional synthesis relies on sacrificial polymers but not easily controlled pores size. Therefore, how to increase porosity and conductivity of carbon nanofibers simultaneously as well as keep their integrity has still deemed as a great challenge [24,25].

Herein, one-dimensional (1D) carbon nanofibers were firstly prepared using polyvinyl alcohol (PVA) and polytetrafluoroethylene (PTFE) as precursors by electrospinning technology (Scheme 1), and the decomposition of PTFE during the carbonization process under Ar atmosphere can lead to the formation of honeycomb-like carbon nanofibers (HCNFs). The specific porous structure of carbon nanofibers can result in the uniformly growth of Bi nanoparticles with smaller size on its surface and successful preparation of Bi/HCNFs nanocomposite. By decorating Bi/HCNFs on screen-printed electrode (SPE), the constructed Bi/HCNFs-SPE exhibits excellent electrocatalytic properties for nitrite oxidation, and can be used for nitrite detection in one drop of aqueous with higher sensitivity, low detection limit, preferable selectivity and long-term stability. Importantly, this electrochemical strategy based on Bi/HCNFs-SPE has also been successfully employed for nitrite determination in real food and environmental samples, and the desired results manifest that this proposed electrochemical sensor could work as a fulfilling sensing platform for highly sensitive analysis of nitrite in food industry and natural environment.

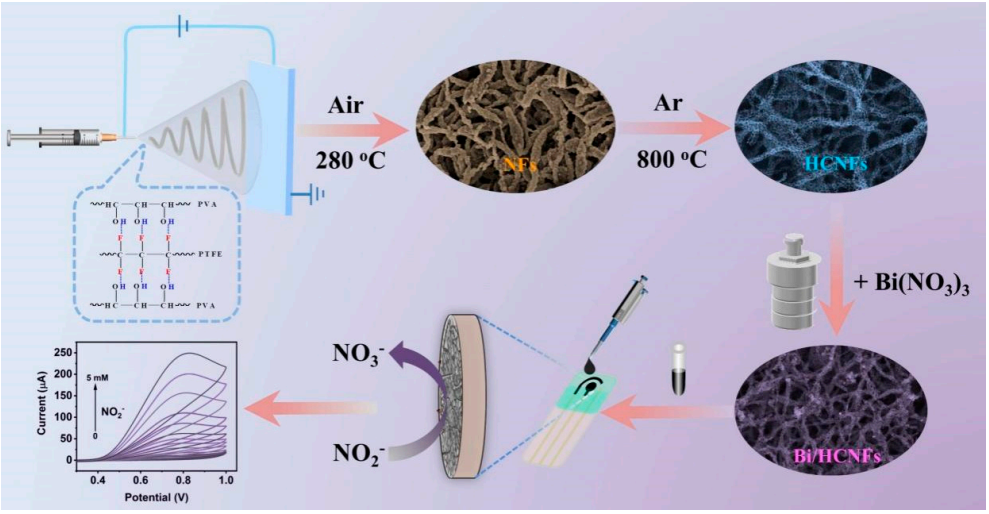

Scheme 1. Schematic illustration of Bi/HCNFs-SPE construction and its electrochemical response to nitrite.

 doi:10.20944/preprints202304.0660.v1

2. Results and discussion

2.1. Synthesis and characterization of Bi/HCNFs

As shown in Scheme 1, polymer nanofibers were firstly prepared with an electrospinning method using PVA and PTEE as precursor. After introducing PTFE into PVA aqueous solution, the formed reversible hydrogen bonding between PVA and PTFE can act as an end-capping agent to regulate the crosslinking degree of viscous solution, benefiting the production of uniformly stable nanofibers (NFs). The as-spun fibers were pretreated in an air atmosphere at 280 °C to prevent PVA pyrolysis and stabilize its 1D nanostructure without collapsing during the pyrolysis process, the color of the fibers changed to brown in this procedure. During the process of annealing at 800 °C for 2 h, the carbonization of PVA formed carbon skeleton and the decomposition of PTFE can create continuous macropores in carbon nanofibers, which leads to the honeycomb-like structure of carbon nanofibers (HCNFs). Then the zeta-potential of HCNFs dispersion has been tested to -10.15 mV. Using HCNFs as the substrate, Bi^{3+} can be electrostatically adsorbed on the HCNFs with negative charge, and subsequently can be reduced to zerovalent Bi atom and grown controllably on its surface through a hydrothermal method, thus finally forming Bi/HCNFs nanocomposites. In this process, the added hydrazine can not only as a reducing agent to reduce Bi^{3+} ions, but also yield N_2 gas to prevent the re-oxidation of Bi NPs in solution. Given that the specific surface area of HCNFs as well as the high affinity of Bi-based materials on nitrogenous compounds, we speculated that the prepared Bi/HCNFs nanocomposite would exhibit high electrocatalytic activity for nitrite oxidation.

Figure 1a-d shows the SEM and TEM image of the as-fabricated HCNFs, it can be seen that the HCNFs are compose of honeycomb skeleton with homogeneous and interlinked hollow holes over the fiber. The high-resolution TEM (HR-TEM) of Figure 1d further illustrates the amorphous property of HCNFs with disordered graphitic ribbons [26]. The SEM and TEM image of Bi/HCNFs are displayed in Figure 1e-h. From Figure 1e, we can clearly see the presence of Bi NPs on HCNFs surface compared with that of HCNFs (Figure 1a). Furthermore, the TEM image of Bi/HCNFs (Figure 1f and Figure 1g) also indicates the uniformly dispersed Bi NPs on HCNFs with an average diameter of 6.86 nm (Figure S1), which is much smaller than reported Bi NPs loaded on CNFs without pores [19], demonstrating the HCNFs can regulate the distribution of Bi NPs and restrain its growth. As a comparation, Bi NPs were also synthesized without the presence of HCNFs, and the larger particles indicate that the HCNFs are pivotal to the formation of ultrasmall nanoparticles (Figure S2), further proving the HCNFs can hinder the growth of Bi NPs. These results all demonstrate the successfully synthesized honeycomb-like carbon nanofibers with smaller Bi NPs, which might endow its higher electrocatalytic activity. Figure 1h shows the HR-TEM image of Bi/HCNFs, and the interlayer spacing of 0.32 nm is attributed to the (012) plane of metal Bi, demonstrating the formed Bi NPs on HCNFs. Besides, the STEM with corresponding energy dispersive X-ray (EDX) elemental mapping images further demonstrate the homogeneous distributed Bi NPs on HCNFs (Figure S3). Figure 1i presents the X-ray diffraction (XRD) patterns of HCNFs and Bi/HCNFs. The distinct diffraction peaks at 27.1°, 37.9°, 39.6°, 48.7° and 64.5° (2θ) are corresponding to the (012), (104), (110), (202) and (122) planes of metal Bi (JCPDS No. 85-1329), respectively. The broad diffraction peak at about 23° reveals the defected or disordered structure of HCNFs [27]. Therefore, the XRD results also confirm the successful formation of Bi NPs on HCNFs (Bi/HCNFs).

Preprints (www.preprints.org) | NOT PEER-REVIEWED | Posted: 21 April 2023 doi:10.20944/preprints202304.0660.v1

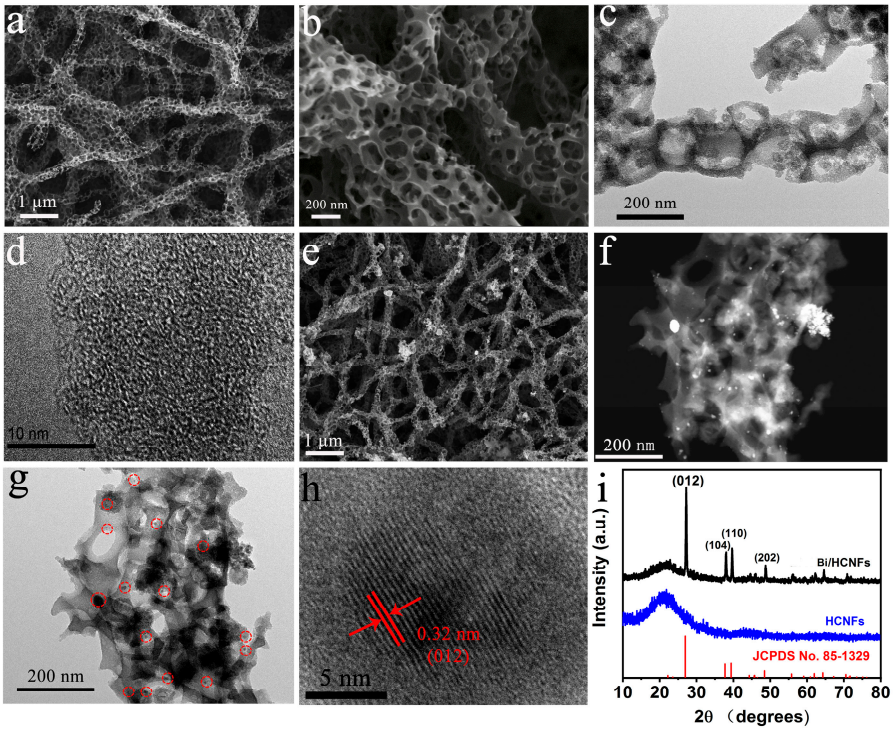

Figure 1. (**a-d**) SEM (**a**, **b**), TEM (**c**) and HR-TEM (**d**) images of HCNFs; (**e-h**) SEM (**e**), TEM (**f**, **g**) and HR-TEM (**h**) images of Bi/HCNFs; (**i**) XRD patterns of HCNFs and Bi/HCNFs.

The elemental composition and chemical state of Bi/HCNFs were then characterized by X-ray photoelectron spectroscopy (XPS). The survey XPS spectrum shown in Figure 2a indicates the presence of Bi, C and O on Bi/HCNFs. The high-resolution XPS spectra of Bi 4f can be deconvoluted into four peaks (Figure 2b). The peak located at 164.2 eV and 159.0 eV is assigned to the $4f_{5/2}$ and $4f_{7/2}$ (Bi_2O_3), respectively. The other two peaks at 163.4 eV and 158.4 eV are belonging to the Bi $4f_{5/2}$ and Bi $4f_{7/2}$ (Bi), respectively [28]. The emergence of few Bi_2O_3 may be attributed to the oxidation of as-prepared material [28]. The C 1s given in Figure 2c reveals three peaks at 283.9 eV, 285.7 eV and 289.0 eV, corresponding to C-C, C-O and C=O respectively. The formation of C=O mainly originated from the oxidation of -OH during the annealing process. The O 1s spectrum illustrated in Figure 2d can be divided into three distinct peaks with binding energy centered at 532.7 eV, 531.5 eV and 529.5 eV, which are ascribed to C-O, -O-C=O and Bi-O bond, respectively. These results further confirmed the Bi NPs are well growth on HCNFs.

Preprints (www.preprints.org) | NOT PEER-REVIEWED | Posted: 21 April 2023 doi:10.20944/preprints202304.0660.v1

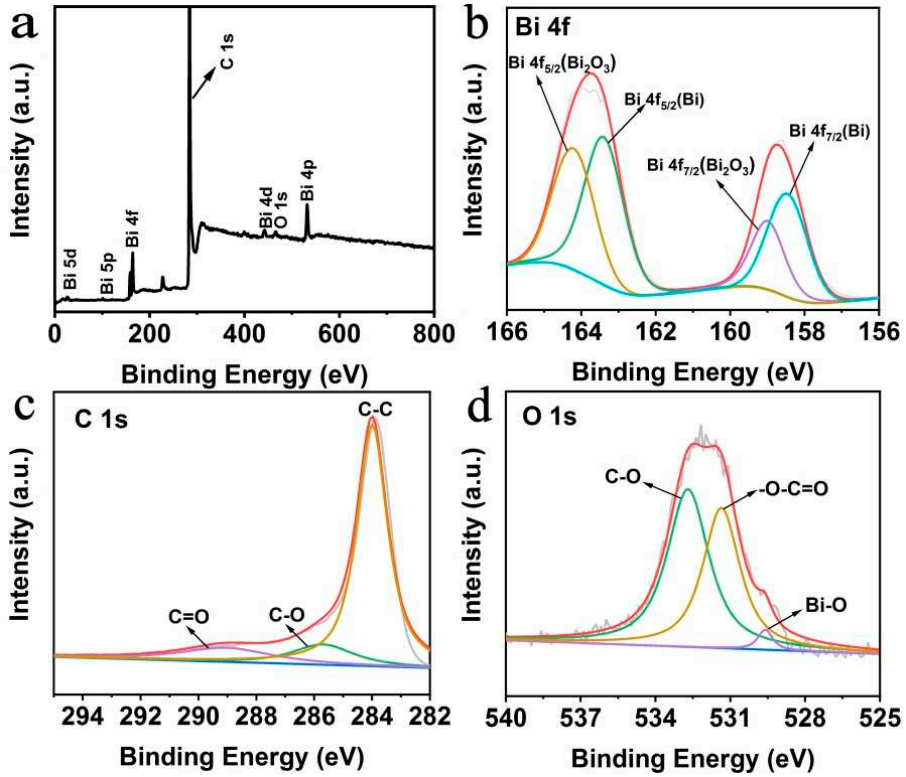

Figure 2. (**a**) XPS survey spectrum of Bi/HCNFs. High-resolution XPS spectrum of Bi 4f (**b**), C 1s (**c**), O 1s (**d**) of Bi/HCNFs.

2.2. Investigation of electrocatalytic behavior of Bi/HCNFs toward NO_2^-

The electrocatalytic performance of as-prepared Bi/HCNFs towards NO_2^- was investigated by locating Bi/HCNFs on glassy carbon electrode (GCE). Figure 3a presents the cyclic voltammograms (CVs) of bare GCE, HCNFs/GCE and Bi/HCNFs/GCE in 0.1 mol·L^{-1} PBS (pH 7.0) before and after the addition of NO_2^- (1 mmol·L^{-1}). From the results, we can see that all three electrodes have an electrochemical response to NO_2^-, and the Bi/HCNFs/GCE has the highest response to NO_2^- oxidation with an anodic peak at 0.79 V, which is lower than that of bare GCE (0.86 V). The bigger response current of Bi/HCNFs/GCE to NO_2^- than that of HCNFs/GCE also indicates the higher catalytic activity of Bi/HCNFs than HCNFs, although both of them have comparative oxidation potential. These results prove that our established Bi/HCNFs possess superior electrocatalytic activity towards the oxidation of NO_2^- to NO_3^-, which can be used as high efficient electrocatalyst to construct electrochemical sensor for NO_2^- detection.

Subsequently, the parameters that may influence the response of Bi/HCNFs to NO_2^-, such as pH and applied potential, were thoroughly investigated. Figure S4 shows the electrochemical response of Bi/HCNFs toward nitrite (1 mmol·L^{-1}) at different pH (from 3.0 to 10.0), we can seen from that the peak current of NO_2^- oxidation presents distinct decrease with pH increasing, and no obvious changed current when pH changing from 6.0 to 10.0 on the response of Bi/HCNFs to nitrite peak oxidation [29]. Hence, a PBS buffer solution with pH=7.0 is selected as the supporting electrolyte in following experiments, and such pH value is beneficial for applications in real food and environment samples. To know the optimal potential to apply to the electrochemical sensor in amperometric analysis, the amperometric current response of Bi/HCNFs with continuous added NO_2^- was carried out at different potentials from 0.70 V to 0.85 V under stirring conditions (Figure S5). The results exhibit the gradually increased current response with the increasing of applied potentials, but a bigger noise signal can be observed at higher potential. Thus, 0.80 V is selected as the optimal potential in the following electrochemical tests.

Preprints (www.preprints.org) | NOT PEER-REVIEWED | Posted: 21 April 2023 doi:10.20944/preprints202304.0660.v1

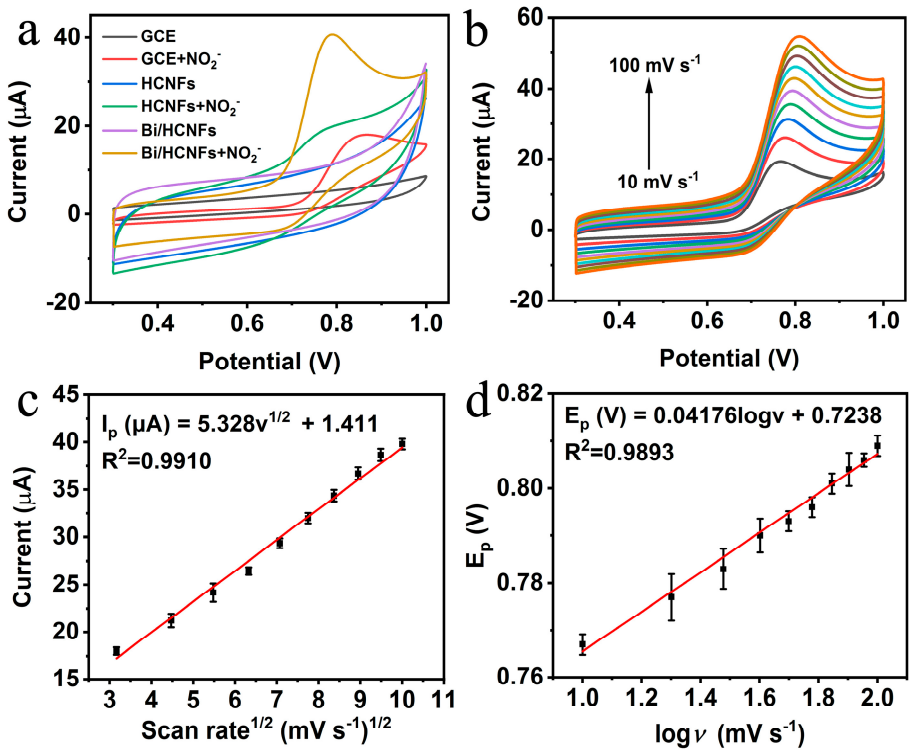

Figure 3. (**a**) CV curves of bare GCE, HCNFs and Bi/HCNFs modified GCE in 0.1 mol·L^{-1} PBS solution (pH 7.0) before and after the addition of NO_2^- (1 mmol·L^{-1}) at a scan rate of 50 mV s^{-1}. (**b**) CV curves of Bi/HCNFs in 0.1 mol·L^{-1} PBS solution (pH 7.0) with the presence of NO_2^- (1 mmol·L^{-1}) at different scan rates. (**c**) Linear relationship between anodic peak current and the square root of scan rate. (**d**) Plots of the oxidative peak potential versus the logarithm of scan rates.

To deeply understand the electrochemical behavior of NO_2^- peak oxidation on Bi/HCNFs, the relationship between the oxidation peaks of NO_2^- and the scan rates (from 10 to 100 mV s^{-1}) was explored in 0.1 M PBS containing 1 mmol·L^{-1} NO_2^-. As shown in Figure 3b, the anodic peak current (I_P, μA) increases with the gradually increased scan rate (v, mV s^{-1}), which is proportional to the square root of scan rate, corresponding equation can be simulated as $I_P = 5.328v^{1/2} + 1.411$ (R^2=0.9910) (Figure 3c). This result manifests that the electrochemical oxidation of nitrite on Bi/HCNFs is a diffusion-controlled irreversible process [14,30]. Additionally, the oxidation peak potential (E_P) also shows a positive shift with the increasing scan rate, and the linear regression equation between E_P (V) and logv can be expressed as $E_P = 0.04176\log v + 0.7238$ (R^2=0.9893) (Figure 3d). Consequently, the number of electrons of this irreversible electrochemical process can be calculated through the following equation, which describes the linear relationship between E_P and logv (eq. (A.1)):

$$E_p = \frac{2.303RT}{2(1-\alpha)n_\alpha F}\log v + K \quad (1)$$

where, n_α represents the number of electron transfer, α is the electro-transfer coefficient, R, T, and F refers to the thermodynamic constant (8.314 J mol^{-1} K^{-1}), thermodynamic temperature (298 K) and Faraday constant (96,485 C mol^{-1}), respectively. α can be calculated to be 0.86 for Bi/HCNFs through Tafel plot. According to the linear equation of E_P vs. logv, the value of n is calculated to be 0.933≈1, indicating the one-electron transfer process of NO_2^- oxidation on Bi/HCNFs is the rate-determining step [31]. So, we speculate that there are three steps in the process of NO_2^- oxidation on Bi/HCNFs: i) NO_2^- in the solution firstly binded on the surface of Bi/HCNFs through complex interaction to form Bi/HCNFs(NO_2^-); ii) the complex Bi/HCNFs(NO_2^-) lose one electron to produce NO_2; iii) NO_2 molecules are involved to the disproportionation reaction and generated NO_2^- and NO_3^-; further electrocatalytic oxidation of NO_2^- occurred to form NO_3^-, thus NO_3^- is the finally possible product.

Preprints (www.preprints.org) | NOT PEER-REVIEWED | Posted: 21 April 2023 doi:10.20944/preprints202304.0660.v1

2.3. Detection of nitrite based on Bi/HCNFs electrode

By locating Bi/HCNFs on the working electrode (WE) of screen-printed electrode (SPE) with Ag/AgCl and carbon as reference electrode (RE) and counter electrode (CE), respectively (Figure 4a), the modified electrode of Bi/HCNFs-SPE was constructed and then used for NO_2^- detection. Such Bi/HCNFs-SPE possesses low cost, simple operation and high stability, as a potential sensing platform for NO_2^- detection. The electrochemical performance of Bi/HCNFs-SPE was firstly investigated in 0.1 mol·L^{-1} PBS solution with the presence of 1 mmol·L^{-1} NO_2^-. As can be seen from Figure S6, an obvious oxidation peak is observed, and the peak current is about four-folds higher than that of bare SPE, indicating the higher sensitive response of Bi/HCNFs-SPE to NO_2^-. Figure 4b shows the CV curves based on Bi/HCNFs-SPE in 0.1 mol·L^{-1} PBS (pH=7.0) with different nitrite contained (from 0 to 5 mmol·L^{-1}). We can see that the current increases gradually with the increasing of nitrite concentration from 0 to 5 mmol·L^{-1}. In order to further evaluate the electrochemical response of Bi/HCNFs-SPE toward NO_2^-, chronoamperometric testing was recorded with the consecutive addition of various NO_2^- under stirring constantly at 0.80 V vs. Ag/AgCl. As shown in Figure 4c, a current response can be observed even with the addition of lower concentration of 0.1 μmol L^{-1} NO_2^-, which increases with the increasing concentration of NO_2^-. The current can keep a steady within 3 s after the addition of NO_2^-, indicating the fast amperometric response of Bi/HCNFs-SPE toward NO_2^-. Figure 4d displays the corresponding calibration curve that from Figure 4c, and gradually increased current (I, μA) with the increasing of NO_2^- concentration (C, mM) can be observed. In the higher concentration range (0.8 ~ 5 mmol·L^{-1}), a corresponding linear equation can be expressed as I = 42.86C + 40.87 (R^2 = 0.9978) with a sensitivity of 634.9 μA mM^{-1} cm^{-2}. In the range of 0.1 ~ 800 μmol·L^{-1}, a linear equation can be calculated to be I = 89.72C + 1.008 (R^2 = 0.9978) with an excellent sensitivity of 1269.9 μA mM^{-1} cm^{-2}, and the corresponding detection limits can be calculated to be 19 nmol·L^{-1} with a signal-to-noise ratio of 3. These results declare that our established Bi/HCNFs-SPE possess higher electrochemical properties toward NO_2^- than most previous reported metal-based electrochemical sensors in Table S1.

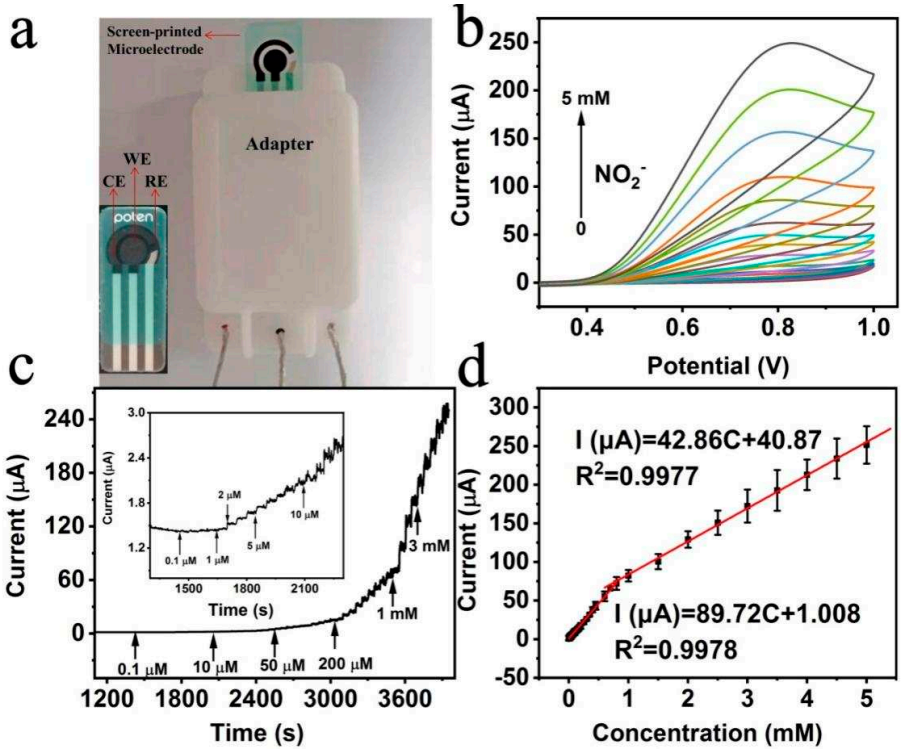

Figure 4. (**a**) The photo of commercial screen-printed electrode. (**b**) CV curves of Bi/HCNFs-SPE in 0.1 mol·L^{-1} PBS (pH 7.0) with different concentrations of NO_2^- ranging from 0 to 5 mmol·L^{-1}. (**c**) Amperometric responses of Bi/HCNFs-SPE with continuous addition of nitrite at 0.80 V vs. Ag/AgCl

(inset: corresponding response at low concentration of NO_2^-). (**d**) Corresponding fitting curves of current response vs. nitrite concentration.

We speculate that these excellent electrochemical properties of Bi/HCNFs-SPE to NO_2^- should be from the special honeycomb-like porous structure of HCNFs, which not only leads to the high surface area of HCNFs, but also the uniformly distributed Bi NPs with smaller size. To demonstrate this, the electrochemical response of Bi NPs loaded on CNFs without porous structure (Bi/CNFs) and Bi NPs without substrate to NO_2^- were also investigated as a comparation. Figure 5a displays the electrochemical response of Bi/HCNFs, Bi/CNFs and Bi NPs to NO_2^-, respectively. The highest response of Bi/HCNFs to nitrite than that of Bi NPs and Bi/CNFs demonstrates the higher catalytic activity of Bi/HCNFs. Based on this, the nitrogen adsorption-desorption isotherm of HCNFs was performed and a mass of mesoprous and macroporous can be seen from the pore size distribution, which leads to the high porosity of HCNFs (Figure S7). In addition, the electrochemical active surface areas (ECSA) of Bi NPs, Bi/CNFs and Bi/HCNFs were compared by measuring the capacitance of the electric double layer (Figure S8a-c), and the result (Figure S8d) indicates that Bi/HCNFs have the largest capacitance of 1.42 mF cm^{-2}, which is 3.3 and 8.6 times than that of Bi/CNFs (0.43 mF cm^{-2}) and Bi NPs (0.165 mF cm^{-2}), respectively. Therefore, all experiment results above mentioned confirm that it is the high specific area of HCNFs and small size of Bi NPs endows the excellent electrochemical performance of Bi/HCNFs for nitrite detection, further demonstrating its great potential applications for constructing electrochemical sensors with higher performance.

2.4. Interference, reproducibility and stability of Bi/HCNFs-SPE and real sample analysis

To demonstrate its practical application, the interference, reproducibility and stability of prepared Bi/HCNFs-SPE for NO_2^- detection were then investigated in detail. As seen from Figure 5b, Bi/HCNFs-SPE exhibits a sharp increase of current response after the addition of NO_2^- (0.1 mmol L^{-1}). However, the added common anions/cations (Na^+, K^+, CO_3^{2-}, SO_4^{2-}, Cl^-) as well as usually coexisted food additives (including glucose, sucrose, nitrate, citric acid, benzoic acid, sodium benzoate) have no influence on the detection of NO_2^-, even with a 10-fold concentration higher than nitrite. The further addition of NO_2^- (0.1 mmol L^{-1}) in the above mixture can also result in a comparable current increasing with the first time added, indicating the excellent selectivity of Bi/HCNFs-SPE to nitrite.

The reproducibility and stability are other key parameters for sensor practical applications. Figure 5c indicates the response of constructed five Bi/HCNFs-SPE toward NO_2^- response (0.1 mmol L^{-1}), and the slight variations with a relative standard deviation (RSD) of 4.6% indicates the good reproducibility of modified electrode based on Bi/HCNFs. Furthermore, the long-term stability of Bi/HCNFs-SPE for nitrite detection was also tested. As shown in Figure 5d, the response current can be maintained to 86% after five weeks of continuous testing, indicating its desirable long-stability in practical application.

Preprints (www.preprints.org) | NOT PEER-REVIEWED | Posted: 21 April 2023 doi:10.20944/preprints202304.0660.v1

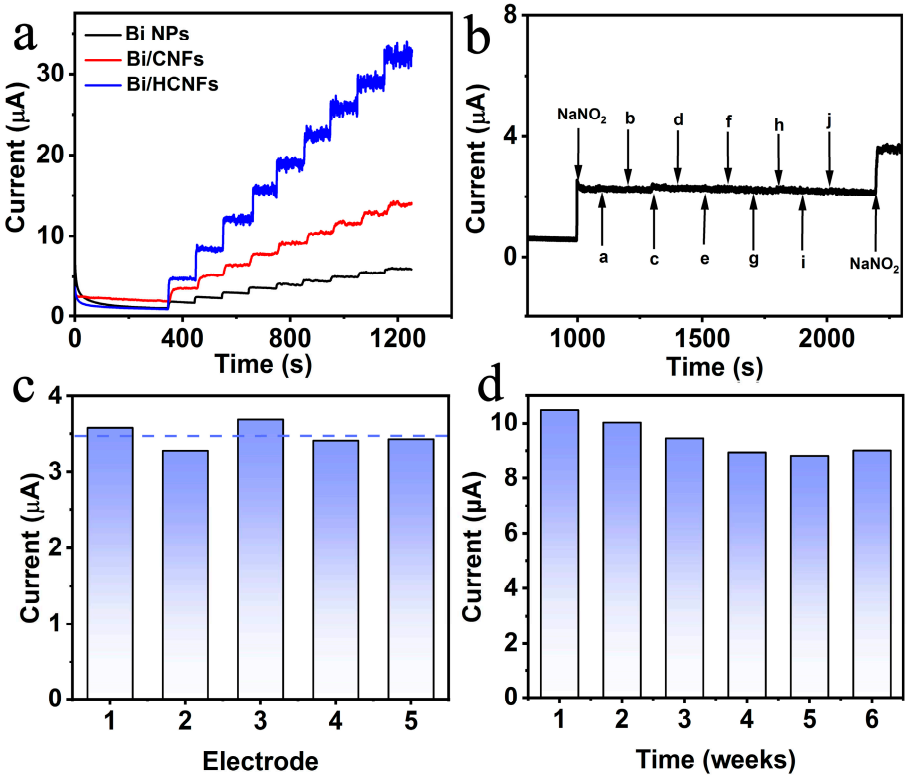

Figure 5. (**a**) The amperometric responses of different electrocatalysts modified GCE with the successive addition of 0.2 mmol L^{-1} nitrite at 0.80 V vs. Ag/AgCl. (**b**) Amperometric responses of Bi/HCNFs-SPE to the successive added 0.1 mmol L^{-1} NO_2^-, 1 mmol L^{-1} Na_2CO_3 (a), Na_2SO_4 (b), K_2CO_3 (c), NaCl (d), Glu (e), sucrose (f), $NaNO_3$ (g), citric acid (h), sodium benzoate (i), benzoic acid (j), and 0.1 mmol L^{-1} NO_2^- in 0.1 mol L^{-1} PBS at 0.80 V vs. Ag/AgCl. (**c**) The amperometric responses toward 0.1 mmol L^{-1} nitrite using five newly prepared Bi/HCNFs-SPE in stirred 0.1 mmol L^{-1} PBS solution (pH 7.0); (**d**) The amperometric responses toward 0.2 mmol L^{-1} nitrite at Bi/HCNFs-SPE with an interval of one week.

The analytical applicability of fabricated Bi/HCNFs-SPE was investigated by monitoring the nitrite concentration in real food and environmental samples. As listed in Table 1, satisfactory recoveries of the electrochemical strategy based on amperometric method in the range of 94%-105% and RSD from 0.4% to 4.9% were obtained with different spiking concentrations of nitrite in tap water, pickles and sausage. To further prove the accuracy of the results obtained from Bi/HCNFs-SPE, UV-vis spectrophotometric method was also adopted to determine the nitrite in same spiked samples, and the comparable results indicate the reliability of constructed Bi/HCNFs-SPE for practical application in complex samples. More interestingly, based on the small size of as-prepared electrode, our well-fabricated disposable SPE also can be used for nitrite detection in one drop of aqueous solution through the cyclic voltammetry method (about 200 μL, Figure S9) with good recoveries between 102%-106% (Table S2). These excellent properties of Bi/HCNFs-SPE accompanied with the advantages of low-cost, convenient operation, quickly-response, demonstrate its potential application in complicated food and environment samples with nitrite contained.

Table 1. Analysis results of real samples conducted utilizing the modified electrode and spectrophotometric method.

Samples	Electrochemical method				Spectrophotometric method		
	Added (μM)	Found (μM)	Recovery (%)	[a]RSD (%)	Found (μM)	Recovery (%)	[a]RSD (%)
Tap water	5.0	4.9	98.0	0.4	4.8	96.0	2.8
	50.0	52.1	104.2	0.8	46.7	93.4	1.6

Preprints (www.preprints.org) | NOT PEER-REVIEWED | Posted: 21 April 2023 doi:10.20944/preprints202304.0660.v1

	500.0	527.1	105.4	1.9	501.6	100.3	0.5
Pickles	5.0	4.9	98.0	0.5	5.3	106.0	2.4
	50.0	50.5	101.0	0.8	49.6	99.2	1.1
	500.0	510.5	102.1	2.1	508.6	101.7	0.1
Sausage	5.0	4.9	98.0	4.9	5.1	102.0	1.4
	50.0	47.1	94.2	1.4	50.8	101.6	1.5
	500.0	511.5	102.3	4.8	513.3	102.7	0.7

Bulleted li[a]RSD: Relative standard deviation.

Materials and Methods

3.1. Reagent and materials

Bismuth nitrate pentahydrate ($Bi(NO_3)_3·5H_2O$), hydrazine hydrate ($N_2H_4·H_2O$), ammonia ($NH_3·H_2O$) were bought from Chengdu Kelong Chemicals (Chengdu, China), polyvinyl alcohol (PVA, MW～67000), polytetrafluoroethylene (PTFE, 120 nm) were obtained from Aladdin Reagent Co., Ltd. (Shanghai, China), glucose (Glu), sucrose, urea, sodium chloride (NaCl), sodium carbonate (Na_2CO_3), sodium sulfate (Na_2SO_4), potassium carbonate (K_2CO_3), citric acid, benzoic acid, sodium benzoate, sodium nitrite ($NaNO_2$), sodium nitrate ($NaNO_3$), sodium dihydrogen phosphate ($NaH_2PO_4·2H_2O$), disodium hydrogen phosphate ($Na_2HPO_4·12H_2O$) were purchased from Aladdin Chemical Reagent Company (Shanghai, China). All above chemicals are analytical grade and without further purification before use.

3.2. Characterizations

X-ray diffraction patterns were obtained from a Shimazu XRD-6100 diffractometer with Cu Kα radiation (40 kV, 30 mA) of wavelength 0.154 nm (Japan). Scanning electron microscopy (SEM) images were collected on GeminiSEM 300 from Carl Zeiss Microscopy GmbH. Energy-dispersive X-ray spectroscopy (EDS) was recorded on Gemini SEM 300 scanning electron microscope (ZEISS, Germany) at an accelerating voltage of 5 kV. Transmission electron microscopy (TEM) images were obtained on using an H-800 electron microscope and an H-8010 scanning system (Hitachi, Japan). X-ray photoelectron spectroscopy (XPS) data were measured on Thermo Scientific K-Alpha with Al Kα radiation. The zeta-potential was conducted on a Malvern Nano ZS90 Zetasizer Nano instrument (Worcestershire, UK). The ultraviolet-visible (UV-Vis) absorption spectra were received on a UV-2900 spectrophotometer.

3.3. Synthesis of HCNFs

PVA was dissolved in the deionized water to prepare PVA solution (15 wt.%) at 60 oC for 3 h with a constant stirring rate. After cooling to room temperature, the PTFE water emulsion (60 wt.%) was added into the above mixture solution and kept vigorously stirring for 3 h. Subsequently, the precursor solution was put in a plastic syringe with a stainless steel nozzle connected with a high-voltage power supply. The electrospinning process was performed with high voltage of 18 kV and 18 cm distance between the needle and aluminum foil collector. After that, the as-spun film was kept in a muffle furnace at 280 °C for 3 h and then calcined at 800 °C at Ar atmosphere with a heating rate of 5 °C min-1 to collect as-fabricated HCNFs nanofibers. For comparison, carbon nanofibers without porous (CNFs) were synthesized with the same procedures except the using of PTFE.

3.4. Synthesis of Bi/HCNFs

The Bi/HCNFs was prepared through a facile hydrothermal method. Typically, HCNFs (1 mg mL^{-1}) were first dispersed into deionized water and then added $Bi(NO_3)_3$ (0.5 $mmol·L^{-1}$) with continuously stirring for 3 h. Next, 3 mL $N_2H_4·H_2O$ (85 wt%) and 1 mL $NH_3·H_2O$ (28 wt%) were injected into the above mixture and kept magnetically stirring. After that, the suspension was carefully transferred into 50 mL Teflon-lined autoclave, which was sealed and heated at 120 °C for 18

h. Subsequently, the as-produced product was thoroughly washed several times with deionized water and acetone, respectively. Finally, the collected black powder was dried at 40 oC under vacuum. However, Bi/CNFs were prepared by using CNFs instead of HCNFs under the same procedure. For comparison, Bi NPs and HCNFs were synthesized with similar procedure without HCNFs and $Bi(NO_3)_3$ used.

3.5. The pretreated of actual samples and spectrophotometric test of nitrite

The tap water was acquired from Sichuan University, which was filtered with a 0.22 μm membrane before testing. The pickle and sausage were purchased from local market. Pickles were firstly crushed into homogenize and 5 g of above samples were dissolved into 50 mL ultrapure water and centrifuged to acquire the supernatant. Sausage was grinded into puree and a part of it (5 g) was added into 150 mL conical flask with adding 80 mL ultrapure water, which was ultrasound for 30 min. Subsequently, mixture was heated at 75 ^{o}C and then cooled to room temperature. Finally, the turbid solution was centrifuged to obtain the supernatant at 10000 r/min. According to the Chinese National Food Safety Standard (GB 5009.33-2016), the food samples were pretreated with 0.1 mol L^{-1} PBS solution (pH 7.0) before measuring.

As a comparison, the nitrite concentrations of real samples were quantified through spectrophotometric method. Generally, a sulfonamide diazide coupled with N-(1-naphthalene)-ethylenediamine dihydrochloride to form a purple azo dye at a pH of 2.0 ~ 2.5. The color agent was prepared by mixing 0.2 g N-(1-naphthyl) ethylenediamine dihydrochloride, 2.0 g sulfonamide, and 5.88 mL H_3PO_4 in 100 mL ultrapure water. After that, 1 mL of spiked sample was reacted with the mixture of 1 mL color agent and 2 mL ultrapure water under dark conditions. It can be quantified by photometric measurements in the wavelength of 400 ~ 700 nm. According to the absorption spectrum, 546 nm was selected as the maximum absorption wavelength to determine nitrite content.

3.6. Electrochemical properties investigation of Bi/HCNFs

The electrochemical properties of Bi/HCNFs were investigated by immobilizing Bi/HCNFs on a glassy carbon electrode (GCE) with the diameter of 3 mm from Shanghai Yuehe Electronic Technology Co., LTD. The screen-printed electrode was purchased from Qingdao Bonaco Technology Co., LTD (POTE, TC201). The blank GCE was firstly polished with α-Al_2O_3 powder (0.05 μm) and then ultrasound with ethanol and deionized water respectively before the modification or direct use. The prepared Bi/HCNFs were dispersed in an ethanol aqueous solution (ethanol/water=3:1) under ultrasonication to form aqueous suspension (5 mg mL^{-1}), then 5 μL of the resulting suspension was dropped on the pretreated GCE surface. For comparison, Bi/CNFs, Bi NPs and HCNFs-modified GCE were prepared with the above process under the same modification quantities. The cyclic voltammetry and chronoamperometry curves were measured using CHI 660E electrochemical analyzer (CHI Instruments, Inc., Shanghai) with a three-electrode system, in which Pt wire as the counter electrode, Ag/AgCl/saturated KCl solution was the reference electrode. The electrolyte solution was 0.1 M PBS solution (pH 7.0).

4. Conclusion

In summary, a honeycomb-like carbon nanofibers (HCNFs) were successfully fabricated with an electrospun method, and the obtained HCNFs can be used as desired substrate for Bi nanoparticles decoration (Bi/HCNFs). The as-fabricated Bi/HCNFs exhibits excellent electrochemical properties toward NO_2^- oxidation, therefore, it can be used for construction electrochemical sensor for NO_2^- detection by locating Bi/HCNFs on a commercial screen-printed electrode (Bi/HCNFs–SPE), which has been successfully used for NO_2^- analysis in complex samples with high sensitivity, excellent selectivity, good anti-interference, and satisfactory stability. The high properties of sensor should be attributed to the unique structure of HCNFs, which can not only enhance the active area of material, but also regulate the growth of Bi nanoparticles, leading to the highly distributed smaller Bi NPs on HCNFs. Notably, the constructed sensor based on Bi/HCNFs can also be used for NO_2^- detection in

sausage, pickles and tap water samples, even in one drop of samples. The obtained satisfactory recoveries for NO_2^- detection indicate Bi/HCNFs–SPE can be used as a promising sensing platform for accuracy analysis of nitrite in the fields of environment and food.

Supplementary Materials: The following supporting information can be downloaded at the website of this paper posted on Preprints.org. Figure S1: particle size distribution histograms of Bi NPs on the surface of HCNFs; Figure S2: STEM image and corresponding elemental mapping images of Bi, C, O for Bi/HCNFs, respectively; Figure S3:The SEM image of Bi NPs (inset of Figure S3 high magnification SEM image); Figure S4: The diagram of CV peak current and pH in the presence of 1 mM NO_2^- ranging from 6.0 to 10.0; Figure S5: The amperometric responses of Bi/HCNFs at different potentials of 0.70-0.85 V vs. Ag/AgCl with successive additions of 0.2 mM nitrite; Figure S6: CV responses of disposable bare SPE and Bi/HCNFs modified SPE in 0.1 M PBS (pH 7.0) with the presence of 1 mM NO_2^-; Figure S7: (a) Nitrogen adsorption-desorption isotherms of HCNFs and (b) its corresponding pore size distribution; Figure S8: CV curves of Bi NPs (a), Bi/CNFs (b) and Bi/HCNFs (c) at different scan rates from 20 to 120 mV s^{-1} in the region without faradic current. (d) Plot of corresponding capacitive current densities of Bi NPs, Bi/CNFs and Bi/HCNFs with scan rates; Figure S9: The photo of commercial screen-printed electrode with a drop of solution containing nitrite (200 μL). Table S1: Comparison of electrocatalytic performance toward nitrite with previous electrochemical sensors; Table S2: Analysis results of trace nitrite in real samples on Bi/HCNFs-SPE through dropping tests (200 μL).

Author Contributions: Conceptualization, F.W., X.Y., J.D. and B.Z.; methodology, validation, F.W. X.Y., J.D. and B.Z.; formal analysis, B.Z. and F.W; investigation, F.W., Y.L., C.Y. and Q.M.; resources, X.Y.; data curation, J.D., B.Z., H.P. and H.W.; writing—original draft preparation, F.W.; writing—review and editing, Y.L., C.Y., Q.M., X.Y., J.D. Y.G. and B.Z.; project administration, J.D. and B.Z.; funding acquisition, J.D. and B.Z. All authors have read and agreed to the published version of the manuscript."

Funding: This work is financially supported by the National Natural Science Foundation of China (Nos.21876117, U1833124 and U1833202) and the Open Research Fund of School of Chemistry and Chemical Engineering, Henan Normal University (No.2021YB05).

Informed Consent Statement: Not applicable.

Data Availability Statement: The data presented in this study are available in the supplementary material.

Conflicts of Interest: The authors declare no conflict of interest.

References

1. Li, X. Ping; J. & Ying, Y. Recent developments in carbon nanomaterial-enabled electrochemical sensors for nitrite detection. *TrAC Trends in Anal. Chem.* **2019**, *113*, 1–12.
2. Wolff, I. A.; Wasserman, A.E. Nitrates, nitrites, and nitrosamines. *Science* **1972**, *177*, 15–19.
3. He, C.; Howes, B.D.; Smulevich, G.; Rumpel, S.; Reijerse, E.J.; Lubitz, W.; Cox, N.; Knipp, M. Nitrite dismutase reaction mechanism: kinetic and spectroscopic investigation of the interaction between nitrophorin and nitrite. *J. Am. Chem. Soc.* **2015**, *137*, 4141-4150.
4. Hegesh, E.; Shiloah, J. Blood nitrates and infantile methemoglobinemia. *Clin. Chim. Acta* **1982**, *125(2)*, 107–115.
5. Yuan,B.; Zhang, J.; Zhang, R.; Shi, H.; Wang, N.; Li, J.; Ma, F.; Zhang, D. Cu-based metal–organic framework as a novel sensing platform for the enhanced electro-oxidation of nitrite. *Sens. Actuators B: Chem.* **2016**, *222*, 632–637.
6. Zhang, J.; Huang, X.; Liu, C.; Shi, H.; Hu, H. Nitrogen removal enhanced by intermittent operation in a subsurface wastewater infiltration system. *Ecol. Eng.* **2005**, *25*, 419–428.
7. Radhakrishnan, S.; Krishnamoorthy, K.; Sekar, C.; Wilson, J.; Kim, S.J. A highly sensitive electrochemical sensor for nitrite detection based on Fe_2O_3 nanoparticles decorated reduced graphene oxide nanosheets. *Appl. Catal. B: Environ.* **2014**, *148-149*, 22–28.
8. Lin, Z.; Xue, W.; Chen, H.; Lin, J.M. Peroxynitrous-acid-induced chemiluminescence of fluorescent carbon dots for nitrite sensing. *Anal. Chem.* **2011**, *83*, 8245–8251.
9. Ma, Z.; Li, J.; Hu, X.; Cai, Z.; Dou, X. Ultrasensitive, specific, and rapid fluorescence turn-on nitrite sensor enabled by precisely modulated fluorophore binding. *Adv. Sci.* **2020**, *7*, 2002991.
10. Zhang, H.; Kang, S.; Wang, G.; Zhang, Y.; Zhao, H. Fluorescence determination of nitrite in water using prawn-shell derived nitrogen-doped carbon nanodots as fluorophores. *ACS Sensors* **2016**, *1(7)*, 875–881.
11. Antczak-Chrobot, A.; Bąk, P.; & Wojtczak, M. The use of ionic chromatography in determining the contamination of sugar by-products by nitrite and nitrate. *Food Chem.* **2018**, *240*, 648–654.

12. Nam, J.; Jung, I.B.; Kim, B.; Lee, S.M.; Kim, S.E.; Lee, K.N.; Shin, D.S. A colorimetric hydrogel biosensor for rapid detection of nitrite ions. *Sens. Actuators B: Chem.* **2018**, *270*, 112–118.
13. Han, Y.; Zhang, R.; Dong, C.; Cheng, F.; Guo, Y. Sensitive electrochemical sensor for nitrite ions based on rose-like AuNPs/MoS_2/graphene composite. *Biosens. Bioelectron.* **2019**, *142*, 111529.
14. Wang, X.; Li, M.; Yang, S.; Shan, J. A novel electrochemical sensor based on TiO_2–$Ti_3C_2T_x$/CTAB/chitosan composite for the detection of nitrite. *Electrochim. Acta* **2020**, *359*, 136938.
15. Wang, F.; Lv, X.; Zhu, X.; Du, J.; Lu, S.; Alshehri, A.A.; Alzahrani, K.A.; Zheng, B.; Sun, X. Bi nanodendrites for efficient electrocatalytic N_2 fixation to NH_3 under ambient conditions. *Chem. Commun.* **2020**, *56*, 2107–2110.
16. Wang, F.; Zhang, L.; Wang, T.; Zhang, F.; Liu, Q.; Zhao, H.; Zheng, B.; Du, J.; Sun, X. In situ derived Bi nanoparticles confined in carbon rods as an efficient electrocatalyst for ambient N_2 reduction to NH_3. *Inorg. Chem.* **2021**, *60*, 7584–7589.
17. Choi, J.; Du, H.L.; Nguyen, C.K.; B. Suryanto, H.R.; Simonov, A.N.; MacFarlane, D.R. Electroreduction of nitrates, nitrites, and gaseous nitrogen oxides: a potential source of ammonia in dinitrogen reduction studies. *ACS Energy Lett.* **2020**, *5*, 2095–2097.
18. Fang, Z.; Wu, P.; Qian, Y.; Yu, G. Gel-derived amorphous BiNi alloy promotes electrocatalytic nitrogen fixation via optimizing nitrogen adsorption and activation. *Angew. Chem. Int. Ed.* **2020**, *60*, 4275–4281.
19. Yin, H.; Li, Q.; Cao, M.; Zhang, W.; Zhao, H.; Li, C.; Huo, K.; Zhu, M. Nanosized-bismuth-embedded 1D carbon nanofibers as high-performance anodes for lithium-ion and sodium-ion batteries. *Nano Res.* **2017**, *10*, 2156–2167.
20. Jeromiyas, N.; Elaiyappillai, E.; Kumar, A.S.; Huang, S.T.; Mani,V. Bismuth nanoparticles decorated graphenated carbon nanotubes modified screen-printed electrode for mercury detection. *J. Taiwan Inst. Chem. E.* **2019**, *95*, 466–474.
21. Li, S.; Yang, Y.; Liu, L.; Zhao, Q. Electron transfer-induced catalytic enhancement over bismuth nanoparticles supported by N-doped graphene. *Chem. Eng. J.* **2018**, *334*, 1691–1698.
22. Wang, J.; Kaskel, S. KOH activation of carbon-based materials for energy storage. *J. Mater. Chem.* **2012**, *22*, 23710.
23. Zhu,Y.; Murali, S.; Stoller, M.; Ganesh, K.J.; Cai, W.; Ferreira, P.J.; Pirkle, A.; Cychosz, K.A.; Thommes, M.; Su, D.; Stach, E.A.; Ruoff, R.S. Carbon-based supercapacitors produced by activation of graphene. *Science* **2011**, *332*, 1537–1541.
24. Wang, P.; Zhang, D.; Ma, F.; Ou, Y.; Chen, Q.N.; Xie, S.; Li, J. Mesoporous carbon nanofibers with a high surface area electrospun from thermoplastic polyvinylpyrrolidone. *Nanoscale* **2012**, *4*, 7199.
25. Xu, Y.; Zhang, C.; Zhou, M.; Fu, Q.; Zhao, C.; Wu, M.; Lei, Y. Highly nitrogen doped carbon nanofibers with superior rate capability and cyclability for potassium ion batteries. *Nat. Commun.* **2018**, *9*, 1720.
26. Yan, J.; Dong, K.; Zhang, Y.; Wang, X.; Aboalhassan, A.A.; Yu, J.; Ding, B. Multifunctional flexible membranes from sponge-like porous carbon nanofibers with high conductivity. *Nat. Commun.* **2019**, *10*, 5584.
27. Zhang, P.; Zou, L.; Hu, H.; Wang, M.; Fang, J.; Lai, Y.; Li, J. 3D hierarchical carbon microflowers decorated with MoO_2 nanoparticles for lithium ion batteries. *Electrochim. Acta* **2017**, *250*, 219–227.
28. Yi, L.; Chen, J.; Shao, P.; Huang, J.; Peng, X.; Li, J.; Wang, G.; Zhang, C.; Wen, Z. Molten-salt-assisted synthesis of bismuth nanosheets for long-term continuous electrocatalytic conversion of CO_2 to formate. *Angew. Chemie Int. Ed.* **2020**, *59*, 20112–20119.
29. Kozub, B.R.; Rees, N.V.; Compton, R.G. Electrochemical determination of nitrite at a bare glassy carbon electrode; why chemically modify electrodes?*Sens. Actuators B: Chem.* **2010**, *143*, 539–546.
30. Wang, S.; Liu, M.; He, S.; Zhang, S.; Lv, X.; Song, H.; Han, J.; Chen, D. Protonated carbon nitride induced hierarchically ordered Fe_2O_3/H-C_3N_4/rGO architecture with enhanced electrochemical sensing of nitrite. *Sens. Actuators B: Chem.* **2018**, *260*, 490–498.
31. Lei, H.; Zhu, H.; Sun, S.; Zhu, Z.; Hao, J.; Lu, S.; Cai, Y.; Zhang, M.; Du, M. Synergistic integration of Au nanoparticles, Co-MOF and MWCNT as biosensors for sensitive detection of low-concentration nitrite, *Electrochim. Acta* **2021**, *365*, 137375.